J Comput Aided Mol Des (2011) 25:1107–1119
DOI 10.1007/s10822-011-9489-y

A computational analysis of the binding mode of closantel as inhibitor of the *Onchocerca volvulus* chitinase: insights on macrofilaricidal drug design

Aldo Segura-Cabrera · Virgilio Bocanegra-García · Cristian Lizarazo-Ortega · Xianwu Guo · José Correa-Basurto · Mario A. Rodríguez-Pérez

Received: 6 May 2011 / Accepted: 8 November 2011 / Published online: 19 November 2011

Abstract Onchocerciasis is a leading cause of blindness with at least 37 million people infected and more than 120 million people at risk of contracting the disease; most (99%) of this population, threatened by infection, live in Africa. The drug of choice for mass treatment is the microfilaricidal Mectizan® (ivermectin); it does not kill the adult stages of the parasite at the standard dose which is a single annual dose aimed at disease control. However, multiple treatments a year with ivermectin have effects on adult worms. The discovery of new therapeutic targets and drugs directed towards the killing of the adult parasites are thus urgently needed. The chitinase of filarial nematodes is a new drug target due to its essential function in the metabolism and molting of the parasite. Closantel is a potent and specific inhibitor of chitinase of *Onchocerca volvulus* (OvCHT1) and other filarial chitinases. However, the binding mode and specificity of closantel towards OvCHT1 remain unknown. In the absence of a crystallographic structure of OvCHT1, we developed a homology model of OvCHT1 using the currently available X-ray structures of human chitinases as templates. Energy minimization and molecular dynamics (MD) simulation of the model led to a high quality of 3D structure of OvCHIT1. A flexible docking study using closantel as the ligand on the binding site of OvCHIT1 and human chitinases was performed and demonstrated the differences in the closantel binding mode between OvCHIT1 and human chitinase. Furthermore, molecular dynamics simulations and free-energy calculation were employed to determine and compare the detailed binding mode of closantel with OvCHT1 and the structure of human chitinase. This comparative study allowed identification of structural features and properties responsible for differences in the computationally predicted closantel binding modes. The homology model and the closantel binding mode reported herein might help guide the rational development of novel drugs against the adult parasite of *O. volvulus* and such findings could be extrapolated to other filarial neglected diseases.

Keywords *Onchocerca volvulus* · Chitinase · Docking · Drug design · Tropical neglected diseases · Molecular dynamics · MM/PBSA

A. Segura-Cabrera (✉) · C. Lizarazo-Ortega
Laboratorio de Bioinformática, Centro de Biotecnología Genómica, Instituto Politécnico Nacional, Boulevard del Maestro esquina Elías Piña, Colonia Narciso Mendoza, 88710 Ciudad Reynosa, Tamaulipas, México
e-mail: asegurac@ipn.mx; aldosegura@gmail.com

A. Segura-Cabrera
Doctorado en Ciencias en Biotecnología, UAM Reynosa Aztlán, Universidad Autónoma de Tamaulipas, Reynosa, México

V. Bocanegra-García
Departamento de Biología Molecular y Bioingeniería, UAM Reynosa Aztlán, Universidad Autónoma de Tamaulipas, Reynosa, México

X. Guo · M. A. Rodríguez-Pérez
Laboratorio de Biomedicina Molecular, Centro de Biotecnología Genómica, Instituto Politécnico Nacional, Boulevard del Maestro esquina Elías Piña, Colonia Narciso Mendoza, 88710 Ciudad Reynosa, Tamaulipas, México

J. Correa-Basurto
Laboratorio de Modelado Molecular-SEPI y Departamento de Bioquímica de la Escuela Superior de Medicina del Instituto Politécnico Nacional, Plan de San Luis y Díaz Mirón s/n, México D.F. 11340, México

Introduction

Onchocerciasis is caused by the infection with the filarial nematode *Onchocerca volvulus* with some 37 million people

infected; some 120 million people are at-risk for infection from onchocerciasis in Africa, and some half a million people in the Americas are also threatened by infection [1]. The accepted treatment for onchocerciasis is Mectizan® (ivermectin), which is mass distributed in most affected countries. Ivermectin exhibits potent microfilaricidal activity against many major filarial parasites in humans; it also has effects on adult *O. volvulus* female worm viability and fertility and marked reductions in the frequencies of male worms [2, 3]. However, the adult worms, which have an average estimated lifespan of 10 years, cannot be killed by the treatment at the standard dose which is a single annual dose aimed at disease control solely in Africa [4, 5]. Hence, new therapeutic targets and drugs are needed to treat and cure this devastating disease in endemic foci of Africa where elimination will not be feasible by using treatment with ivermectin alone and because in this continent, ivermectin is being distributed annually.

Historically, there have been research efforts to develop or discover new macrofilaricides, however, few are promising and are not useful for mass treatment hitherto. The most recent advances for a new macrofilaricidae are the discovery of a new chemical class of synthetic anti-helminthics, the amino-acetonitrile derivatives [6]. They seem to have a novel mode of action involving a unique, nematode-specific clade of acetylcholine receptor subunits. The amino-acetonitrile derivatives were efficacious against various species of livestock-pathogenic nematodes, well tolerated, and of low toxicity to mammals [6]. Closantel, a well-known veterinary antihelmintic, was identified a new activity, it is as a potent and specific competitive inhibitor of the chitinase from *O. volvulus* (OvCHT1) and other filarial chitinases, an activity not previously, reported for this compound [7].

Previously, Wu et al. [8] had proposed that chitinases expressed by infective stages of the filarial nematodes may play a role in ecdysis during post-infective development. Chitinases have been detected in several parasitic organisms, including *Plasmodium* spp, *Leishmania, Trypanosoma* and filarial nematodes, all of which are transmitted by arthropods, suggesting a relationship between chitinase and parasite transmission [9]. Immunization with a recombinant chitinase expressed by the microfilariae of *Brugia malayi* induces partial protection against microfilaremia in Mongolian Jirds [10]. In addition, DNA vaccination with the chitinase gene Ov-CHT1, a L3 specific chitinase from *Acanthocheilonema viteae,* induced protection against the infective L3 of *O. volvulus* in mice [8, 11].

OvCHT1 (a member from the family 18 chitinases) was found to express only in the L3 stage [8, 9]. Other chitinases had been found in developing eggs in the uterus of the adult worm and in the microfilariae [8, 9]. Therefore, the inhibition of these enzymes may represent new drug targets against *O. volvulus*. In a study aiming at discovering inhibitors of Ov-CHT1, four (Levofloxacin, Lomefloxacin, Dexketoprofen and Closantel) out of 1,514 drugs of the Johns Hopkins Clinical Compound Library collection, were identified as hits; however, only closantel showed potent inhibition ($IC_{50} = 1.6 \pm 0.08$ μM) [7]. Closantel inhibited molting of *O. volvulus* L3 to L4 in culture at a concentration of 100 μM, and was specific for the filarial chitinases when compared with chitinases from other parasitic species and the human chitotriosidase isoforms [7]. However, the specific binding mode of closantel as inhibitor of OvCHT1 is still yet unknown. In the present paper, the tridimensional (3-D) structure of OvCHT1 was modeled. Then, the complexes of closantel on either OvCHT1 or human chitinase were determined by docking simulations, and analyzed by molecular dynamics simulations, binding free-energy and free-energy decomposition analyses. Such information of closantel-OvCHT1 complexes obtained from the present study could aid in screening and designing new macrofilaricides or selective inhibitors for chemotherapy against *O. volvulus* and the findings expanded to the discovery of new drugs against other filarial neglected diseases.

Materials and methods

Sequence retrieving, analysis, and homology modeling

The amino acid sequence of the OvCHT1 with accession number Q25615 was retrieved from Uniprot database [12]. The Basic Local Alignment Search Tool (BLAST) [13] found several human homologous proteins with known 3-D structures located at Protein Data Bank (PDB) which were used as the template in homology modeling of OvCHT1. A comparative sequence analysis between the mammalian and filarial chitinases was then performed. The amino acid sequences of *Mus musculus, Rattus norvegicus, Pan troglodytes, Brugia malayi,* and *Wuchereria bancrofti* with accessions codes: NP_082255, NP_001073157, XP_514112.2, P29030, and AAF66988, respectively, were retrieved from non-redundant database of NCBI while those of human, *Loa-loa*, and *O. volvulus* were retrieved from the PDB (code: 1HKK), Broad Institute (by Broad Institute-BLAST searching), and Uniprot (accession code: Q25615), respectively. The multiple sequence alignment of chitinases sequences was performed by T-coffe program [14]. The final multiple sequence alignment was edited using structural information and secondary structure analysis which was carried out in the PSIPRED server [15]. The 3-D structures of three human chitinases (PDB codes: 1HKK, 1WAW, and 3FXY) were selected as templates. The 3D-model of the OvCHT1 was built based on templates with the MODELLER 9v7 program [16, 17]. The

quality of homology model was verified employing the PROCHECK[18], ANOLEA [19], and ProSA [20] programs. RMSD values between OvCHT1 model and human templates were calculated by the use of the Chimera program [21]. The best model, according to the lowest MODELLER objective function and validated by the PROCHECK, ANOLEA, and ProSA programs, was further refined by energy minimization and MD simulations.

Refinement of homology model by molecular dynamics simulation

The selected 3-D model was refined by MD simulations with the parallel version of GROMACS 4.5.3 [22] in an Amber force field (amber99sb). The model was solvated in a cubic box with the size of 1.5 nm. The TIP3 water model was used to create aqueous environment, periodic boundary conditions were applied in all directions, and the system was neutralized by adding 4 Na^+ ions to replace the water molecules. The water molecules and ions alone were subjected to energy minimization and MD simulations (a step time of 1 fs) for 20 ps to freeze the 3-D OvCHT1 structure. Therefore, the whole system was minimized and subjected to 100 ps equilibration. All above simulations were performed at constant temperature and pressure with a non-bonded cut-off of 14 Å, and all bond lengths were constrained with the LINCS algorithm [23]. The SETTLE algorithm [24] was applied to constrain the geometry of water molecules, and the pre-equilibrated system was subsequently used for MD simulations during 10 ns. The particle mesh Ewald method [25] was employed for the electrostatic interactions. The integration time-step was 2 fs, with the neighbor list being updated every fifth step by using the grid option and a cut-off distance of 12 Å. The snapshots were collected at every 5 ps and analyzed with GROMACS analysis tools [22]. The lowest potential energy conformation was selected from the 10 ns MD simulation trajectory and further refined by energy minimization for molecular docking. The energy minimized average structure calculated from the equilibrated trajectory system at 10 ns was evaluated for quality determination of protein geometry and structure folding reliability. Subsequently, the dynamic behavior and structural changes of the protein were analyzed by the calculation of total energy and the RMSD values. The refined model was evaluated with the ANOLEA [19] and ProSA [20] programs.

Molecular docking

The AutoDock Vina (Vina) [26] docking package was used for ligand flexible docking simulations. The structures of the templates and the refined model of OvCHT1 were setup as the receptors for docking protocol. Before docking, small ligands and water molecules were removed manually from the templates. The structure of closantel was obtained from Pubchem (http://pubchem.ncbi.nlm.nih.gov/) database. The allosamidin molecule was retrieved from the co-crystal structure with human chitinase (PDB code: 1HKK) [27]. Thus, closantel and allosamidin were used as ligands for docking protocol (Fig. 1). The hydrogens and charges on receptors and ligands were assigned with the Chimera program [21]. The pdbqt files for docking simulations were generated using the AutoDock Tools interface [28, 29].

The method of Troot and Olson [26] and the template 1HKK, that corresponds to the complex between allosamidin and human chitinase, were used in the docking protocol to select the search spaces and to determine the size of search spaces, respectively. Thus, we started with the experimentally bound allosamidin ligand structure and created the minimal rectangular parallelepiped, aligned with the coordinate system that includes it. Then, their sizes were increased by 5 Å in each of the three dimensions until the largest size of search spaces was obtained, to allow that allosamidin binding pose was consistent with experimentally data reported for the 1HKK structure.

The size of search spaces in each dimension (x, y, and z) was 22 Å, with its center in −8.88, 0.00, and 17.99 for x, y and z, respectively. Thus, the search space was large

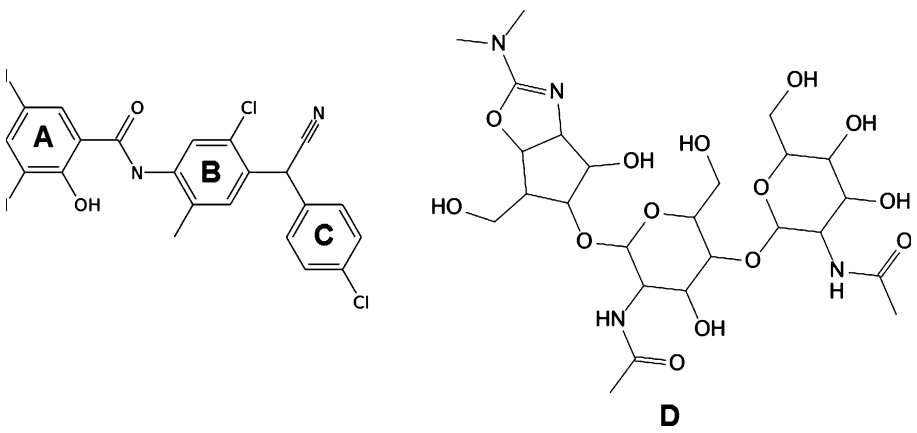

Fig. 1 Structure of closantel. **A**, **B**, and **C** corresponds to the three heteroaromatic systems: 3,5-diiodosalicylic acid, 5-chloro-2-methylaniline, and 4-(chlorophenyl) acetonitrile, respectively. **D** corresponds to structure of allosamidin molecule

enough for the ligands to rotate, as suggested elsewhere [30]. The other Vina default optimization parameters were maintained for docking simulation.

Consensus scoring

It is well-known that the use of multiple and different function scoring (consensus scoring) improves the results of docking studies. Thus, the best complexes according to Vina predictions were subjected to re-scoring with programs X-score [31] and DrugScore [32] using default parameters.

Molecular dynamics and binding free-energy analysis of protein–ligand complexes

The MD simulations of selected protein–ligand complexes were performed with AMBER 11.0 package and AMBER ff99 force field. The force field parameters for closantel were generated by general AMBER force field (gaff) [44] using Antechamber program. To ensure overall electroneutrality of the system, appropriate number of counter ions Na+ ions was added to the most electronegative areas around the protein. The entire complex was subsequently solvated in a box of TIP3P water molecules with a margin of 15.0 Å in each direction from the solute [45]. The particle mesh Ewald (PME) [46, 47] was applied to calculate long-range electrostatic interactions. The cutoff distance for the long-range electrostatic and the van der Waals (vdW) energy terms were set at 8.0 Å. SHAKE algorithm was used to constrain all covalent bonds involving hydrogen atoms [48], allowing for an integration time step of 2 fs. To avoid edge effects, the periodic boundary conditions were applied in MD simulation.

For equilibration, the whole systems were successively minimized by 2,500 steps of steepest descent method following 5,000 steps of conjugated gradient method, while restraining the rest using a force constant of 500, 10, and 0 kcal/mol Å^2, respectively. Then each system was gradually heated from 0 to 300 K over a period of 50 ps and maintained at 300 K with a coupling coefficient of 1.0/ps with a force constant of 1.0 kcal/mol Å^2 on the complex. Each system was again equilibrated to a free simulation for 1000 ps. Finally, a production run for 75 ns was performed using NPT ensemble at 300 K with 1.0 atm pressure. During the MD simulation process, coordinates were collected every 10 ps. The minimization and equilibrations were performed on Argentum cluster at Centro Nacional de Supercómputo, México. All the periodic boundary PME simulations were performed using pmemd.cuda on an Intel Core i7-980x 3.33 Ghz Linux workstation (6 CPUs) with 12 Gb RAM, (2x) NVIDIA Geforce GTX460 and (1x) NVIDIA Geforce GTX580.

For each system, free energy calculations were performed for 4000 snapshots extracted from the last 40 ns stable MD trajectory using MMPBSA approach. For each snapshot, the free energy was calculated for each molecular species (complex, protein, and ligand), and the binding free energy was computed by the standard formula:

$$\Delta G_{bind} = G_{\text{complex}} - \left(G_{\text{protein}} + G_{\text{ligand}}\right) \quad (1)$$

In which, the ΔG bind is given by:

$$\Delta G_{bind} = \Delta G_{\text{MM}} + \Delta G_{\text{solv}} - T\Delta S \quad (2)$$

The molecular mechanics energy including the electrostatic and van der Waals interactions is given by:

$$\Delta G_{MM} = \Delta G_{ele} + \Delta G_{vdw} \quad (3)$$

The solvation free energy was composed of the polar and the nonpolar contributions by:

$$\Delta G_{solv} = \Delta G_{pol} + \Delta G_{nonpol} \quad (4)$$

ΔG_{pol} could be obtained using PBSA module of the AMBER package. The ΔG_{nonpol} term was determined by:

$$\Delta G_{nonpol} = \gamma \text{SASA} + b \quad (5)$$

where γ represents the surface tension and b a constant. They were set at 0.0072 kcal/mol Å^2 and 0, respectively. SASA, the solvent accessible surface area (Å^2), was determined using the linear combination of a pairwise overlaps model. The value of the exterior dielectric constant was set to 80, and the internal dielectric constant was set to 1. The conformational entropic contribution ($T\Delta S$) was estimated for 50 snapshots taken from the trajectories by using the mmpbsa_py_nabnmode module implemented in Amber Tools 1.5. The evaluation of the contribution of each residue to the binding free energy was conducted by free energy decomposition.

Lastly, the ability of the MMPBSA to reproduce the experimental affinities for closantel-OvCHT1 was evaluated. Experimental affinities were derived from published inhibition constants *K*i according to Gloeckner et al. [7].

The experimental binding energies are calculated by:

$$\Delta G_{exp} = RT\ln Ki. \quad (6)$$

Results and discussion

Template selection and sequence analysis

The search of OvCHT1 homologous sequences, with tridimensional structure and deposited in the PDB, was performed using the NCBI protein BLAST program [13]. The BLAST of OvCHT1 showed highest sequence identity (42%) to five human chitinases (1GUV, 1LG1, 1HKK, 1WAW, and 3FXY) [27, 33–35] suggesting that they are

the most suitable templates for homology modeling. Only structures with high resolution were selected to build a homology model for OvCHT1. The selected structures were 1HKK, 1WAW, and 3FXY which had resolution of 1.85, 1.75, and 2.0 Å, respectively. The comparative analysis between filarial chitinases and homologous mammalian chitinases was performed by using the multiple sequence alignment (Fig. 2) of filarial and mammalian chitinases. The sequence analysis showed that most of the key regions for the recognition of chitin and allosamidin inhibitor are conserved in filarial chitinases while in some other regions there is a difference between filarial and mammalian chitinases, for example, the replacements of Trp by Tyr in position 99, Met by Phe in position 356, Tyr by Thr in position 190, and Met by Thr in position 300. However, two significant sequence changes on the filarial chitinases were noticed: 1) an insertion of extra segment between positions 70 and 71, and 2) a deleted segment that corresponds to those residues between 144 and 151 positions on the mammalian chitinases. The extra segment in OvCHT1 was defined as an insertion when considering the result of analysis on the secondary structure and the 3D structure.

Homology modeling and quality assessment of the model

The structure-based sequence alignment depicted in Fig. 2 was used to build a 3-D model of OvCHT1. MODELLER-9v7 [16, 17] was used to generate fifty 3-D models of OvCHT1 based on human chitinases (PDB ID: 1HKK, 1WAW, and 3FXY) as templates. The RMSD of the homology model was calculated by structural superposition of model with three templates on Chimera and was found to be 0.271 Å (1HKK), 0.265 Å (1WAW), and 0.382 Å (3FXY), respectively, which reflected a high structural similarity in the tridimensional structures. RMSD values of ~0.5 Å from alpha carbons occurs in independent X-ray crystallographic determinations of the same protein [36, 37]. Thus, the low RMSD values of the homology model were a clue for a model of acceptable quality.

The quality of the 3-D OvCHT1 obtained by homology modeling was evaluated independently by the PROCHECK (implemented in the Swiss-model server) [38], ANOLEA [19], and ProSA [20], programs. The results of Ramachandran plot produced by PROCHECK showed a homology model with good stereochemical quality, which was supported by the following values of 91.7% of residues in most favored regions, 7.6% in additional allowed regions, and 0.6% in generously allowed regions. The overall G-factors (acceptable between 0 and 0.5) produced by PROCHECK was 0.06, also suggesting a homology model of good quality. In addition, after several iterative rounds of alignment correction, the energetic evaluation performed by ANOLEA and ProSA showed the regions with high energy. These results suggested that some residues (Glu 38, Trp 70a, 70d, Ser 211, Trp 212, Glu 213, Gly 227, Glu 228, Thr 229, Ser 230, Gly 231, and Thr 232) in the homology model do not have favorable energetic environment. Furthermore, to improve the energetic environment of these residues in the 3-D OvCHT1, MD simulations was performed to obtain a refined 3-D model.

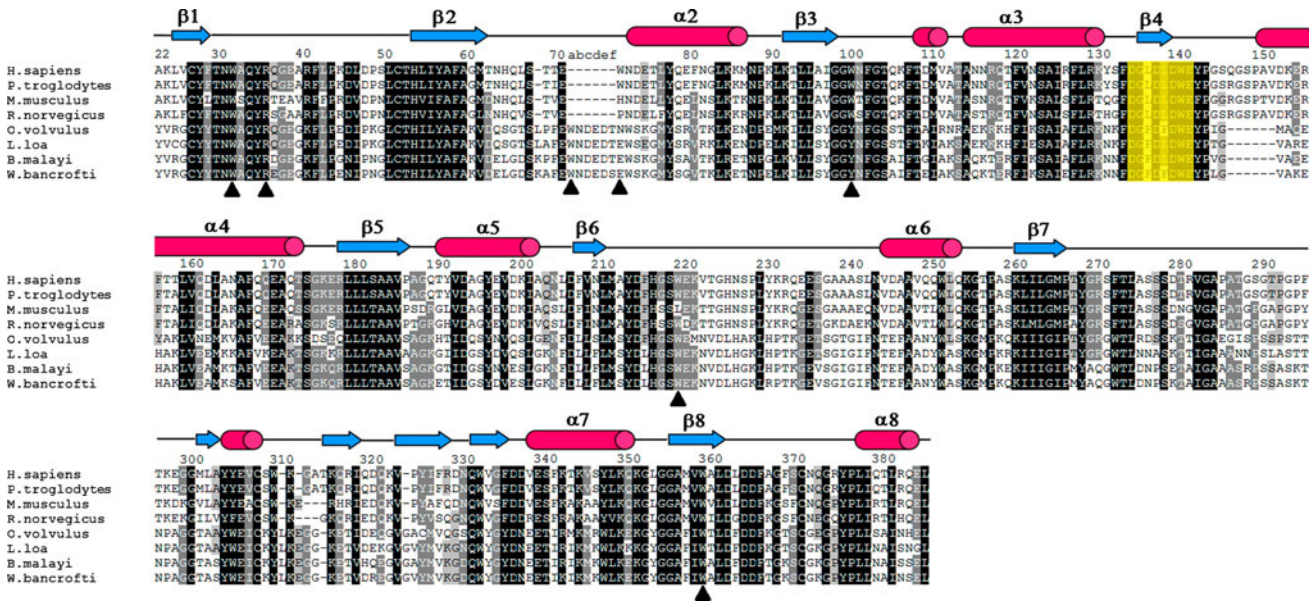

Fig. 2 Sequence alignment of mammalian and filarial chitinases generated by t-coffee algorithm [14]. Secondary elements using PSIPRED [15] are also shown. The DxxDxDxE motif observed in all family 18 chitinases is highlighted in *yellow*. Aromatic residues outlining the binding cleft in chitinases are indicated by *filled triangles*

Refinement of homology model by molecular dynamics simulation

The selected model was subjected to MD simulation for 10 ns in order to assess the stability of the model and to find the energetically favorable structure for further docking study. The variation in the RMSD of structures relative to the initial structures was ~ 2 Å after 4.5 ns of simulation, whereas the RMSD values did not changed significantly after 5 ns of simulations as shown in Fig. 3, indicating that the employed simulation time meets the requirement to obtain an equilibrium structure during the MD simulations of the OvCHT1. The most energetically favorable conformation was selected at the 10 ns MD simulation which was then evaluated by ANOLEA and ProSA programs. ANOLEA and ProSA use knowledge-based mean force potentials to analyze the compatibility of the residues with their environment in initial 3-D model and the selected homology model from MD simulation. It can be seen in Fig. 4 that the ANOLEA energetic profile of the refined model, after MD simulation, fits better than the one from initial model, and also there were few residues with high energy profiles after MD simulation indicating a proper fold of refined homology model. The analysis of ProSA Z-score showed that MD refined model had a better Z-score (−9.01) than that of the initial 3-D model (−8.66), and was closer to Z-score from the template structure (−9.86). All evaluations suggested that an appropriate homology model for OvCHT1 had been obtained for further protein–ligand interaction studies.

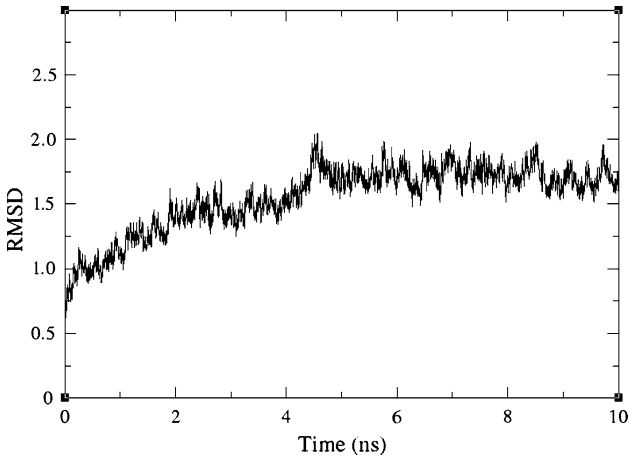

Fig. 3 Backbone root mean square deviation (RMSD) of the model during the simulation

Structural features of OvCHT1 model

The homology model possesses the typical $(\beta/\alpha)_8$ barrel fold in the core domain as found in the family 18 chitinase structures as reported elsewhere [39–42], and an α/β domain, which are involved in the outlining of the binding-site (Fig. 6d). It also contains two conserved disulfide bonds, Cys 26–Cys 51 and Cys 307–Cys 370 [43]. Besides, OvCHT1 contains the sequence motif *DXXDXDXE*, which lies on strand β4 (Fig. 2). Structural and biochemical analysis have shown that the glutamate 140 is the main residue responsible of the OvCHT1 catalysis [33, 42, 44, 45]. The neighboring Asp 138 plays a key role in orienting the N-acetyl group of the sugar at −1 sub-site for nucleophilic attack on the anomeric carbon and stabilizes the formed oxazolinium ion intermediate. Mutation of either of these residues affects its catalytic activity [44, 45].

The comparison of the OvCHT1 model in relation to templates showed that the extra segment, between residues 70 and 71, belongs to the loop located between strand β2 and helix α2. This loop's protrude allows an increase groove character of the binding-site, in particular at the −3 sub-site level. Likewise, the deleted segment corresponding to the region between positions 144 and 151 in human chitinase belongs to the loop located between strand β4 and helix α4, causing a shortening of the loop.

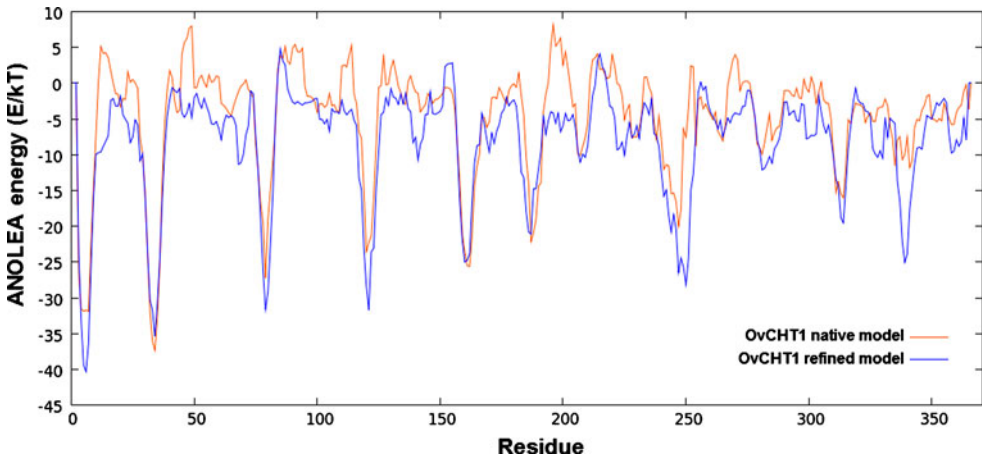

Fig. 4 The ANOLEA [19] energetic profile of refined model (OvCHT1 native model: *blue line*) and the initial model (OvCHT1 refined model: *orange line*)

Thus, the extra segment between positions 70 and 71, and the changes in amino acids produced subtle differences in the binding site of OvCHT1 (Fig. 6) which could be exploited in the future for the rational design of new potent filarial inhibitors.

Molecular docking

To better understand the specificity of closantel for OvCHT1, docking studies on the OvCHT1 model and human chitinase structure were carried out using the Vina program. The structure of human chitinase (1HKK) in complex with allosamidin [27] was used to define the size of search spaces where the dockings were performed. The method of Trott and Olson [26] was adapted to define the size of search space. The conformational and positional RMSD values between the docked binding mode and the experimental binding mode for allosamidin docked into the human chitinase structure was 0.289 and 0.857 Å, respectively, indicating high similarity between predicted and experimental binding mode. The use of a different template did not affect the results of the docking for human chitinases (Fig. 5). For example, the conformational and positional RMSD values for the 1 WAW template were 1.002 and 1.545 Å, respectively. These values are similar to those of 0.987 and 1.703 Å, respectively for the 3FXY template. Thus, the search space was large enough to allow that the ligand rotated as it had been suggested elsewhere [30]. This protocol was then applied to dock closantel into the binding site of human chitinase and into the OvCHT1 model.

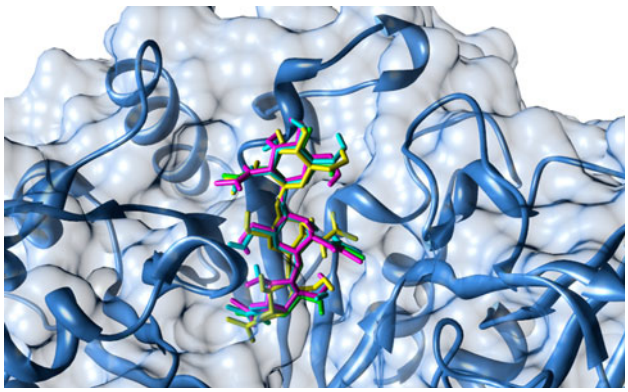

Fig. 5 Result of the docking search spaces using different human chitinase structures. Allosamidin in color *green* correspond to the conformation observed in crystal structure 1HKK; in color *cyan* correspond to the results using 3FXY structure; in color *yellow* correspond to the results using 1WAW structure, and in color *magenta* correspond to the results using 1HKK structure

The results of docking experiments showed that closantel binding to OvCHT1 is dominated by one conformation. The closantel structure is constituted from three heteroaromatic systems: 3,5-diiodosalicylic acid (Fig. 1A), 5-chloro-2-methylaniline (Fig. 1B), and 4-(chlorophenyl) acetonitrile (Fig. 1C) [7]. The analysis of the docked structure of closantel with OvCHT1 showed orientation on −1, −2, and −3 sub-sites forming interactions with residues of binding site similar to those observed in chitinase-allosamidin complexes from crystallography experiments (Fig. 6a) [27, 33, 45, 46]. In contrast, in the human chitinase binding site, two binding conformations were preferred by closantel. The first one showed similar orientation and interactions that the predicted for OvCHT1 (Fig. 6b), and the second one showed that closantel is oriented and interacts with residues of the −1, +1, and +2 sub-sites (Fig. 6c). The analysis of interactions of closantel with residues of the −1, +1, and +2 sub-sites showed that its 4-(chlorophenyl) acetonitrile moiety interacts with the residues Phe58, Asp138, Glu140, Tyr212, and Trp358. The 5-chloro-2-methylaniline and 3,5-diiodosalicylic acid aromatic systems showed interactions with Trp99, Asp213, Arg269, and Trp218, which are conserved in the mammalian chitinases (Fig. 2).

The binding energy of docked poses for closantel with human chitinase was −9.9 kcal/mol at the conformation 1

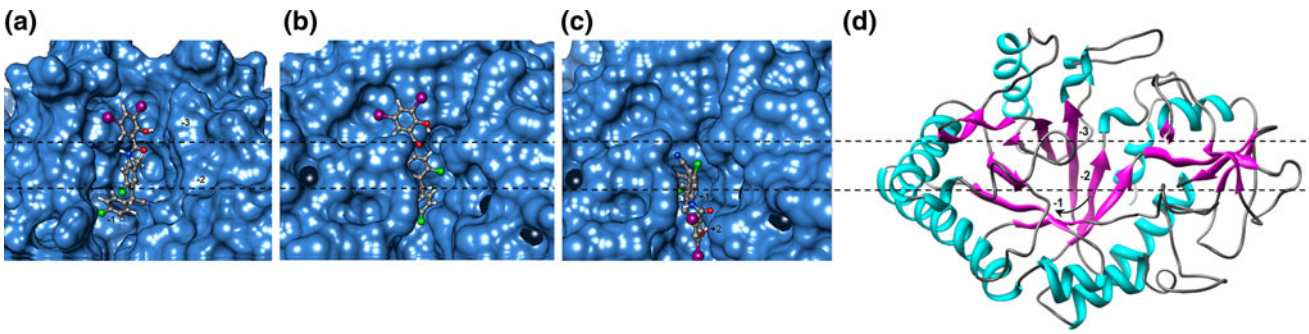

Fig. 6 Orientation and interaction of closantel into chitinase binding site predicted by Vina. **a** closantel-OvCHT1; **b** Pose1, and **c** Pose2, respectively. **d** Structural elements of the constructed OvCHT1 model, where α-helices and β-strands are indicated by *cyan* and *magenta* colors, respectively. The *dotted lines* represent the separation of the sub-sites from the chitinase binding site. The image was produced with Chimera [21]

(Pose1) and −10.9 kcal/mol at the conformation 2 (Pose2). For the closantel-OvCHT1 complex the binding energy was −9.9 kcal/mol. The re-scoring of the 3 complexes with X-score [31] and DrugScore [32] showed similar results suggesting that closantel is an unspecific inhibitor (Table 1). Therefore, the analysis of the scoring of the predicted poses aforementioned showed that docking protocol was not able to distinguish closantel as a specific inhibitor of OvCHT1.

Molecular dynamics of protein–ligand complexes

According to docking and the function re-scoring analyses there were no differences in specificity of closantel towards human chitinase and OvCHT1. Then, a 75 ns MD simulations, and free-energy calculations for each of three complexes selected by docking experiments in a full water solvated box were performed. Thus, the strategy was to improve the binding energies of closantel, taking into account the flexibility of the receptor and identifying the most favored conformation into the binding site of 3-D OvCHT1, which would explain the closantel specificity towards OvCHT1.

In order to explore the stability of the three systems and the guarantee of the sampling method, we analyzed the RMSD from the starting structure (Fig. 7). The Fig. 7 showed that the three systems reach equilibrium after ∼15 ns. However, the conformation1-human chitinase (Pose1) system showed a fluctuation at 45 ns, and then it flattens out after that. The analyses of root-mean-square fluctuation per residue for the three systems are showed in the Fig. 8. As expected, the main backbone fluctuations occur in the loop regions. The closantel-OvCHT1 system showed two loops with high fluctuations that correspond to the extra segment between positions 70 and 71 and the loop that includes residues in positions between 211 and 244 (Fig. 8). According with docking predictions only the first one is involved in the closantel recognition while the second is located far away from the binding-site. Thus, the visual inspection of extra segment between positions 70 and 71 showed that is reorganized in response to conformational adjustments of closantel at the binding-site. However, such conformational change does not affect its role in closantel recognition.

On the other hand, the protein structures of closantel-human chitinase systems share similar RMSF distributions and dynamic features, except in two loops (Fig. 8) which are located between positions 99 and 108, and 175 and 179, respectively. Both systems showed high fluctuations of the loop that include the residues from positions 147 to 151; specifically, Gly in the position 148 shows the major fluctuation value. Moreover, these fluctuations are huge in the conformation2-human chitinase (Pose2) bound system and it appears to be related with the high fluctuations showed by the loop between 175 and 179 positions because both flanked the alfa-4 helix. The visual inspection of this loop (residues 147–151) showed that it moves away from

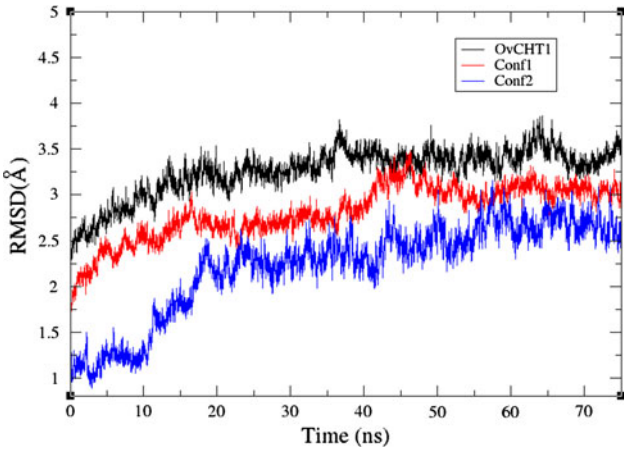

Fig. 7 Backbone root mean square deviation (RMSD) during the simulation of the three complexes

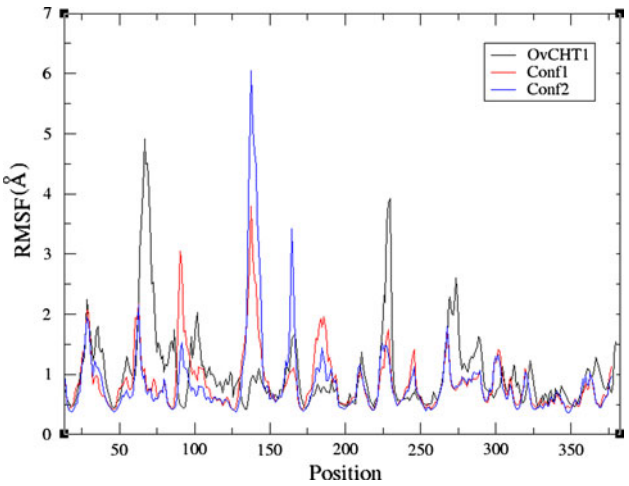

Fig. 8 RMSF of the protein Cα atom for each the three systems

Table 1 Results of docking and re-scoring analyses

Complex	Function scoring		
	Vina [26] (kcal/mol)	X-score [31] (−logKd)	DrugScore [32] (unit free)
Closantel-OvCHT1	−9.9	7.89	−319575
Closantel-Human (Pose1)	−9.9	7.96	−362225
Closantel-Human (Pose2)	−10.9	8.16	−318691

binding site suggesting that this binding mode of closantel destabilize this region. For the Pose1 system, the loop between positions 99 and 108 showed high fluctuation. The visual inspection of this region reveals conformational changes in response to closantel binding; specifically this conformational change produces that this loop switch its orientation from the −2-sub-site to −3-subsite causing the displacement of the loop between 67 and 71 positions far away from the binding-site and corresponds to the fluctuation observed at 45 ns (Fig. 7). Despite of such rearrangement, the loop between positions 99 and 108 is still involved in the closantel recognition.

In order to show the conformational changes and location of closantel during the MD simulations of the three systems, comparison between the initial conformation and location of closantel with a representative structure extracted from the clustering of last 5 ns MD simulations were performed (Fig. 9). The Pose1 system showed no drastic displacements into binding-site maintaining its interactions with residues at −1, −2, and −3 sub-sites (Fig. 9b). The most significant movement observed was the light twist of 4-(chlorophenyl) acetonitrile moiety towards the α/β domain. Thus, closantel in Pose1 system interacts with the residues Trp31, Phe58, Trp99, Tyr212, Asp213, Tyr267, Arg269, and Trp358. In opposite to Pose1 system, the Pose2 system showed a drastic rearrangement into binding-site of human chitinase changing its orientation from −1, +1, and +2 sub-sites to −2, and −3 sub-sites (Fig. 9c). The results for closantel-human chitinase systems suggest that the preferred conformation of closantel into binding-site is the conformation 1, with its 4-(chlorophenyl) acetonitrile moiety packs towards the −1 sub-site, the 5-chloro-2-methylaniline and 3,5-diiodosalicylic acid moieties, interacting with residues from −2 and −3 sub-sites, respectively. In closantel-OvCHT1 system, closantel showed a displacement from the −1, −2, and −3 sub-sites to −2, and −3 sub-sites avoiding that closantel interacts with residues from −1 sub-site (Fig. 9a). Closantel interacts mainly with the residues from the −2 and −3 sub-sites such as Trp31, Tyr34, Arg35, Trp70a, Asn100, Tyr267, Arg269, Asp295, Thr300, and Phe362. Although, closantel-OvCHT1 and closantel-human chitinase systems showed similar interaction patterns during MD simulations, the main differences involved residues from −2 and −3 sub-sites which some of them are not conserved between filarial and mammalian chitinases (Fig. 2). This is the case of residues in positions 70a, 300, and 362. The side chain of residue Trp70a is oriented towards −3 sub-site and interacts with the 3,5-diiodosalicylic acid moiety. The change of Met by Thr in position 300 represents a reduction of the size of side chain and the steric hindrance which seems to contribute to the complete displacement of closantel towards −2 and −3 sub-sites of OvCHT1 binding-site. The change of Leu by Phe at the position 362 represents an increase of the size of side chain allowing the Phe362 to reach the −2 sub-site and interact with closantel. Furthermore, the visual inspections showed that in Pose1 system the side chains of Leu362 and Met300 are oriented face to face avoiding the side chain of Leu362 is oriented to −2 sub-site. Meanwhile, in OvCHT1 the small side chain of Thr300 is not able to interact with Phe362 allowing that its side chain is oriented to −2 sub-site.

We found that the subtle differences in the binding site of OvCHT1 and human chitinases, mainly in the −2 and −3 sub-sites, are related to closantel specificity and that these findings could be exploited to develop novel macrofilaricidal drugs.

Binding free-energy analysis

In order to gain more insights into the specificity of closantel towards OvCHT1, the comparative analysis of binding free energies using MM-PBSA method for the three protein–ligand systems aforementioned was performed (Table 2). The ability of the MM-PBSA method to reproduce the experimental affinities reported for closantel-OvCHT1 was evaluated. Then, a comparative analysis between calculated binding free energy and experimental-derived binding free energy was performed. The calculated binding free energy was lower than that derived from the experiment. That could have been caused by the low accuracy of entropic calculation. However, the MM-PBSA method is able to rank closantel as a much better binder for OvCHT1 than for human chitinase. In addition, the results showed that there was a large difference for the calculated binding free energy between closantel-OvCHT1 and closantel-human chitinase systems. Such difference in binding free energy was estimated to be 12 kcal/mol which implied a change in the *K*i of approximately eight orders of magnitude which is consistent with the observations of Gloeckner et al. [7]. They reported that closantel did not affect the human chitinase even at high concentration. Hence, the calculated binding free energies are compatible with the experimental ones. The detailed analysis suggests that major contributions favorable to binding are vdW and electrostatic energies, whereas polar solvation energies opposed the binding. The nonpolar solvation energies contribute slightly favorable. In addition, the entropy contribution for closantel-OvCHT1 system is higher than that of other systems. In particular, the differences in the entropy values mostly arise from the vibrational entropy term from the complexes and receptors. The differences could be explained bearing in mind the presence of the highly mobile extra segment between positions 70 and 71; this segment is key to the closantel specificity but its conformational changes also suggest an increase in the

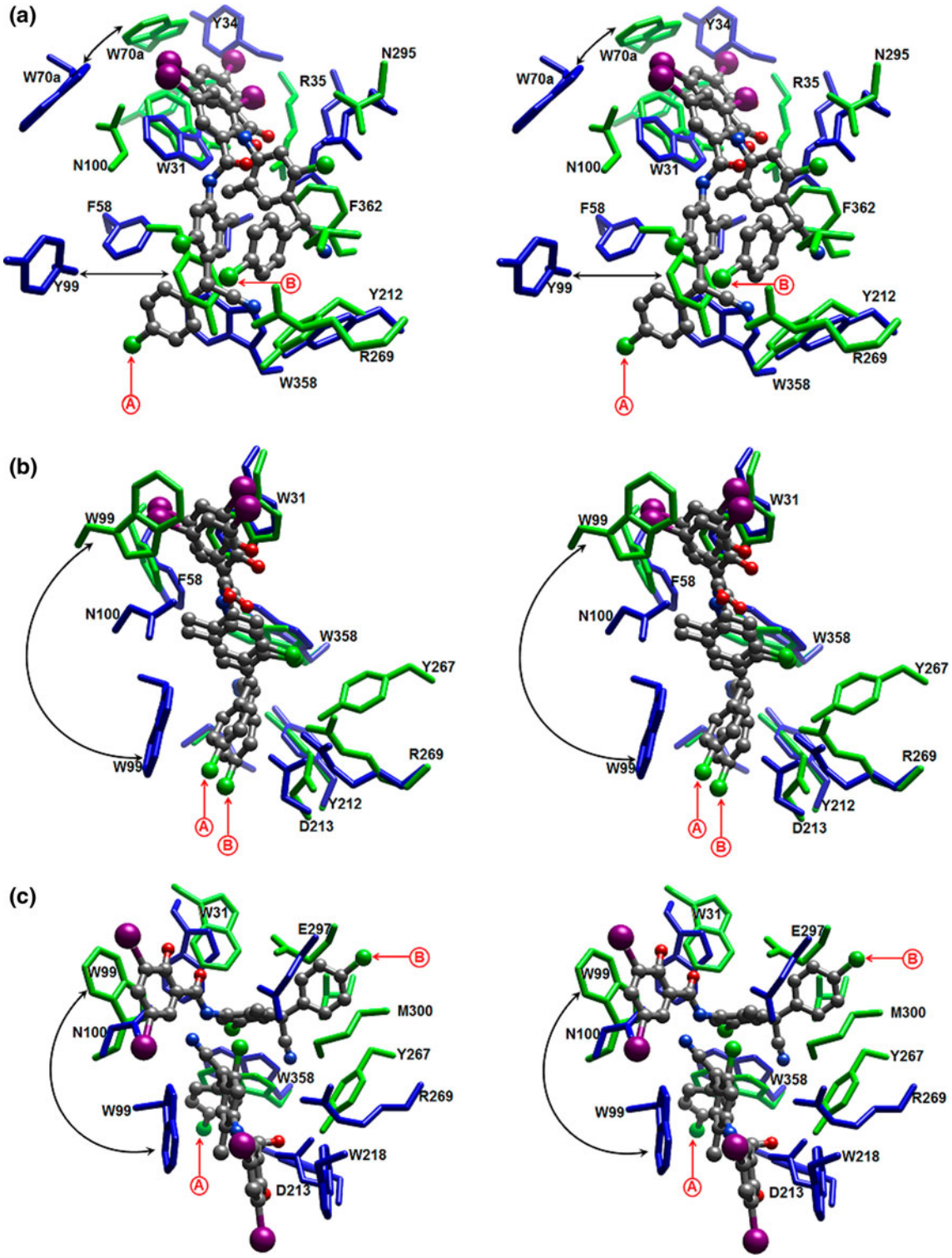

Fig. 9 Stereo view of the comparison between the initial conformation and location of closantel with a representative structure extracted from the clustering of last 5 ns MD simulations; **a** corresponds to closantel-OvCHT1 system, and **b** and **c** to Pose1 and Pose2 systems, respectively. *A* and *B* in color *red* represent the closantel conformations predicted by docking and from the MD simulations, respectively. The residues in color *blue* correspond to those that interact with closantel predicted by docking. The residues in color *green* correspond to those that interact with closantel extracted from the clustering of last 5 ns MD simulations. The *arrows* represent the change of residue orientation in response to closantel binding

Table 2 Binding free-energy calculation for each system, all units are in kcal/mol. The values in parenthesis represent the standard error

System	ΔG_{ele}	ΔG_{vdw}	ΔG_{nonpol}	ΔG_{pol}	ΔH	$-\Delta TS$	$\Delta G_{bind,\ calc}$	$\Delta G_{bind,\ exp}$
OvCHT1	−12.5723	−47.7843	−3.9188	32.7241	−31.5479	19.3404	−12.2075 (0.08)	−8.6252
Pose1	−7.1866	−40.2649	−3.1678	25.2180	−25.4004	25.4209	0.0205 (0.07)	n.d.
Pose2	−6.3773	−37.3895	−3.0353	25.4999	−21.3025	24.3112	3.0087 (0.08)	n.d.

n.d. not determined [7]

entropy of the OvCHT1 system. Despite this produces higher entropy contribution for closantel-OvCHT1 system, its enthalpy term is much lower than that of other systems suggesting that although the entropy contribution is important for binding, the binding free energy makes sense only in the complex relationship among these contributions; therefore closantel-OvCHT1 complex possesses a stronger binding affinity than others complexes (Table 2). Thus, the major differences in binding energies to closantel binding are given by the contribution of van der Waals and electrostatic energies suggesting that the specificity of closantel for OvCHT1 is dominated, primarily, by shape complementarity and, secondly, by electrostatic forces.

To further elucidate the key residues responsible for the energetic differences of closantel binding and examine their contribution, the binding free energy was decomposed on per residue with the MMPBSA method. Figure 10 depicts the important residues for closantel binding identified by the free energy decomposition.

The comparison of the contribution of residues to closantel binding suggests that three residues (31, 99, and 267) contribute with larger energies in the three complexes, and five residues (35, 70a, 295, 300 and 362) also contribute for the closantel-OvCHT1 complex. It is interesting that all those important residues for OvCHT1 binding are a mix of polar and hydrophobic residues, which can form strong van der Waals interactions with closantel.

In closantel-OvCHT1 complex, the side chain of Arg35 forms two hydrogen bonds with the oxygen atoms from hydroxyl and carbonyl groups of the 3,5-diiodosalicylic acid moiety, respectively. Therefore, Arg35 have stronger interaction energy with the inhibitors, especially the electrostatic and van der Waals interactions (−9.511 kcal/mol and −1.503, respectively). The residues Trp70a, Asn295, Thr300, and Phe362 contribute larger energies (Fig. 10). The visual inspection reveals that Asn295, Thr300, and Phe362 make van der Waals contacts with 4-(chlorophenyl) acetonitrile and 5-chloro-2-methylaniline moieties, while Trp70a makes van der Waals make contacts with 3,5-diiodosalicylic acid moiety. The van der Waals energies of these four residues are −1.646, −1.338, 1.342 and −2.08 kcal/mol, respectively. Then, we can conclude that the electrostatic contribution of Arg35 and van der Waals interactions of aforementioned residues at −2 and 3 sub-sites plays an important role in the binding affinity of closantel towards OvCHT1.

Gloeckner et al. [7] used a retro-fragment protocol to produce a set of closantel fragment analogues and found that analogue 7 (fusion of 3,5-diiodosalicylic acid and 4-(chlorophenyl) acetonitrile systems; Fig. 1A–C) showed similar potency to closantel ($IC_{50} = 5.8 \pm 0.3$ μM) and the remainder of fragment analogues showed low potency. However, it is worth noting that after analogue 7, the potency decreases in relationship to the presence of the 3,5-diiodosalicylic acid moiety, $IC_{50} = 33$, 47 μM, for 6 (Fig. 1A, B) and 2 analogues (Fig. 1A), respectively. On the contrary, the 8 (Fig. 1B, C), 5, 4, and 3 analogues which do not have the 3,5-diiodosalicylic acid moiety, showed the lowest potency ($IC_{50} = 67$, 106, 143, and 200, respectively; all units in μM). These findings about the importance of 3,5-diiodosalicylic acid moiety in closantel and analogues activities have led to consider this moiety as lead fragment to develop more potent and specific OvCHT1 inhibitors as reported elsewhere [47]. Moreover, on the light of our structural results, we can suggest that the interactions between 3,5-diiodosalicylic acid moiety and residues at −2 and 3 sub-sites are anchoring the closantel molecule to OvCHT1 biding site, and thus, playing an important role for closantel specificity.

In order to examine consistence of the results of molecular dynamics and free-energy analysis, we performed a re-docking and re-scoring analysis using a representative receptor structure from the clustering of the trajectories of the last 5 ns MD simulation (Table 3). The results showed that using a receptor structure that take into account the changes induced upon ligand binding it is able to identify the preferred conformation and discriminate to closantel as better binder for OvCHT1 than that of the human chitinase. Then, providing the "correct" receptor conformation, the accuracy of docking and scoring analysis was improved, as it was suggested elsewhere [48].

Conclusions

We used a combined computational approach to gain insight into the structural basis of specificity and inhibition mechanism of closantel as inhibitor of OvCHT1. A

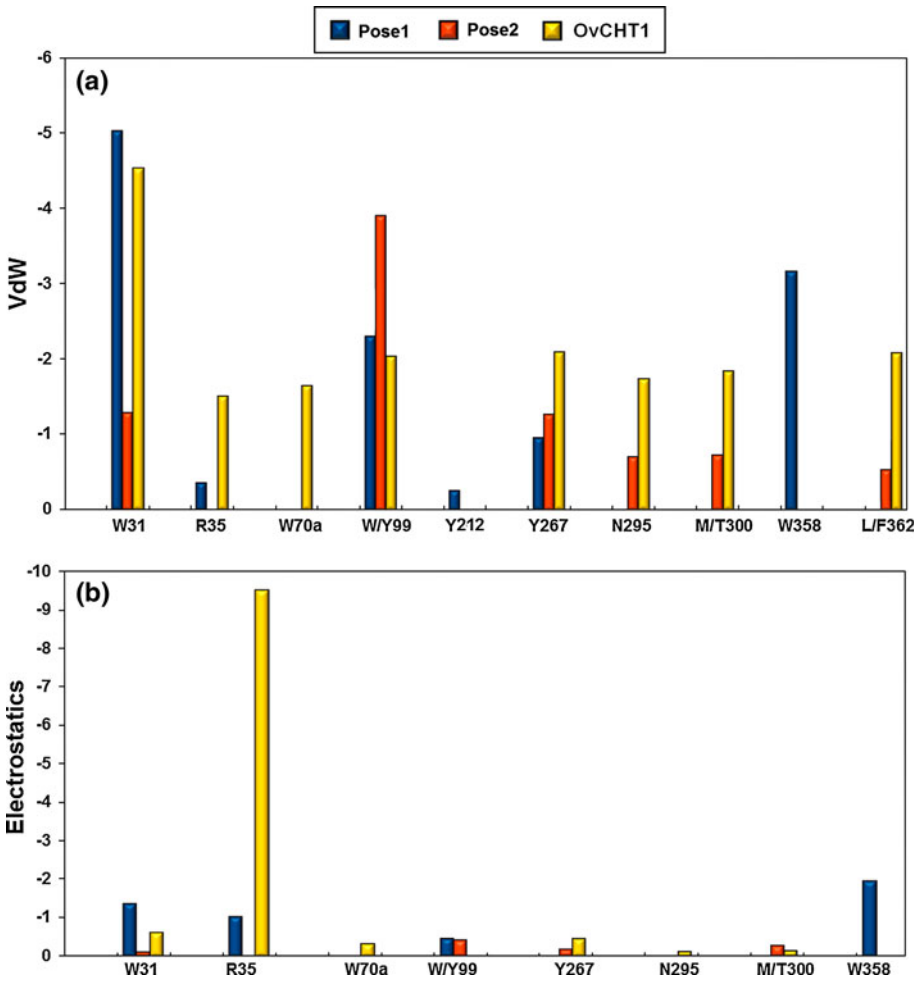

Fig. 10 Comparison of energetic contributions of residues in the binding-site for each system: **a** vdW and **b** electrostatic contributions

Table 3 Results of re-docking and re-scoring analyses using a representative receptor structure from the clustering of the trajectories of the last 5 ns MD simulation

Complex	Function scoring		
	Vina [26] (kcal/mol)	X-score [31] (−logKd)	DrugScore [32] (unit free)
Closantel-OvCHT1	−10.4	7.45	−284772
Closantel-Human (Pose1)	−7.5	6.65	−209261
Closantel-Human (Pose2)	−7.4	6.75	−198169

structural model for OvCHT1 was, for the first time, developed, and used to document the molecular interaction of OvCHT1 with closantel. Structural and sequence analysis of human chitinase and OvCHT1 revealed differences in their binding site. The extra segment of OvCHT1 between positions 70 and 71 belongs to the −3 sub-site that makes structural changes in the groove character and electrostatics of the binding-site, which are important properties for closantel binding. The first docking and consensus scoring results using the modeled structure of OvCHT1 were not able to discriminate to closantel as a specific inhibitor of OvCHT1. Accordingly, by performing 75 ns of MD simulations and calculating free-energy for the complexes predicted by docking, the closantel binding energies were optimized favoring the correct ranking of closantel as inhibitor of OvCHT1. Furthermore, this was confirmed by performing re-docking and re-scoring analyses concluding that the receptor flexibility is key for closantel recognition. The decomposition of binding free energy per residue indicated the van der Waals interactions are the main driving force for the specificity and binding mode of closantel into OvCHT1 binding-site. Also, the energy decomposition revealed that the most favorable contributions to closantel specificity towards OvCHT1 resulted from Arg35, Trp70a, Asn295, Thr300 and Phe362. These findings explain the differences observed in the specificity for both chitinases.

Although experimental validation of the interaction mechanism between closantel and OvCHT1 is further

needed, the findings of the present *in silico* study may help to guide the experimental methods, so that they can complement each other, reducing long term trial studies and technical difficulties arisen from drug-targeting studies. Hence, it is proposed that compounds having similar parent structure/scaffold with modified functional groups might modulate the biological activity of filarial chitinases in a similar manner as closantel**;** such compounds can be considered potential macrofilaricidal candidates.

Acknowledgments The authors thank the Centro Nacional de Supercomputo, México for providing the access to the "Argentum" cluster, Thomas R. Unnasch for critical reading on an earlier draft, Cesar Millán-Pacheco and Nina Pastor for very valuable comments and suggestions. Mario A. Rodríguez-Pérez and Xianwu Guo hold a scholarship from Comisión de Operación y Fomento de Actividades Académicas of Instituto Politécnico Nacional-México.

References

1. Basanez MG, Pion SD, Churcher TS, Breitling LP, Little MP, Boussinesq M (2006) PLoS Med 3(9):e371
2. Cupp EW, Cupp MS (2005) Am J Trop Med Hyg 73(6):1159
3. Cupp EW, Duke BO, Mackenzie CD, Guzman JR, Vieira JC, Mendez-Galvan J, Castro J, Richards F, Sauerbrey M, Dominguez A, Eversole RR, Cupp MS (2004) Am J Trop Med Hyg 71(5):602
4. Basanez MG, Pion SD, Boakes E, Filipe JA, Churcher TS, Boussinesq M (2008) Lancet Infect Dis 8(5):310
5. Diawara L, Traore MO, Badji A, Bissan Y, Doumbia K, Goita SF, Konate L, Mounkoro K, Sarr MD, Seck AF, Toe L, Touree S, Remme JH (2009) PLoS Negl Trop Dis 3(7):e497
6. Kaminsky R, Ducray P, Jung M, Clover R, Rufener L, Bouvier J, Weber SS, Wenger A, Wieland-Berghausen S, Goebel T, Gauvry N, Pautrat F, Skripsky T, Froelich O, Komoin-Oka C, Westlund B, Sluder A, Maser P (2008) Nature 452(7184):176
7. Gloeckner C, Garner AL, Mersha F, Oksov Y, Tricoche N, Eubanks LM, Lustigman S, Kaufmann GF, Janda KD (2010) Proc Natl Acad Sci USA 107(8):3424
8. Wu Y, Adam R, Williams SA, Bianco AE (1996) Mol Biochem Parasitol 75(2):207
9. Wu Y, Egerton G, Underwood AP, Sakuda S, Bianco AE (2001) J Biol Chem 276(45):42557
10. Wang SH, Zheng HJ, Dissanayake S, Cheng WF, Tao ZH, Lin SZ, Piessens WF (1997) Am J Trop Med Hyg 56(4):474
11. Harrison RA, Wu Y, Egerton G, Bianco AE (1999) Vaccine 18(7–8):647
12. Magrane M, Consortium U (2011) Database (Oxford) 2011: bar009
13. Altschul SF, Gish W, Miller W, Myers EW, Lipman DJ (1990) J Mol Biol 215(3):403
14. Notredame C, Higgins DG, Heringa J (2000) J Mol Biol 302(1): 205
15. Bryson K, McGuffin LJ, Marsden RL, Ward JJ, Sodhi JS, Jones DT (2005) Nucleic Acids Res 33(Web Server issue):W36
16. Eswar N, Webb B, Marti-Renom MA, Madhusudhan MS, Eramian D, Shen MY, Pieper U, Sali A (2007) Curr Protoc Protein Sci Chap 2:Unit 2 9
17. Sali A, Blundell TL (1993) J Mol Biol 234(3):779
18. Luthy R, Bowie JU, Eisenberg D (1992) Nature 356(6364):83
19. Melo F, Devos D, Depiereux E, Feytmans E (1997) Proc Int Conf Intell Syst Mol Biol 5:187
20. Wiederstein M, Sippl MJ (2007) Nucleic Acids Res 35(Web Server issue):W407
21. Pettersen EF, Goddard TD, Huang CC, Couch GS, Greenblatt DM, Meng EC, Ferrin TE (2004) J Comput Chem 25(13):1605
22. Van Der Spoel D, Lindahl E, Hess B, Groenhof G, Mark AE, Berendsen HJ (2005) J Comput Chem 26(16):1701
23. Hess BBH, Fraaije J, Berendsen HJC (1997) J Comput Chem 18(12):10
24. Miyamoto SK PA (1992) J Comput Chem 13(8):11
25. York DY W (1994) J Chem Phys 101(4):3
26. Trott O, Olson AJ (2010) J Comput Chem 31(2):455
27. Rao FV, Houston DR, Boot RG, Aerts JM, Sakuda S, van Aalten DM (2003) J Biol Chem 278(22):20110
28. Sanner MF (1999) J Mol Graph Model 17(1):57
29. Sanner MF, Duncan BS, Carrillo CJ, Olson AJ (1999) Pac Symp Biocomput 401
30. Morris GM, Huey R, Lindstrom W, Sanner MF, Belew RK, Goodsell DS, Olson AJ (2009) J Comput Chem 30(16):2785
31. Wang R, Lai L, Wang S (2002) J Comput Aided Mol Des 16(1):11
32. Velec HF, Gohlke H, Klebe G (2005) J Med Chem 48(20):6296
33. Fusetti F, von Moeller H, Houston D, Rozeboom HJ, Dijkstra BW, Boot RG, Aerts JM, van Aalten DM (2002) J Biol Chem 277(28):25537
34. Rao FV, Houston DR, Boot RG, Aerts JM, Hodkinson M, Adams DJ, Shiomi K, Omura S, van Aalten DM (2005) Chem Biol 12(1):65
35. Olland AM, Strand J, Presman E, Czerwinski R, Joseph-McCarthy D, Krykbaev R, Schlingmann G, Chopra R, Lin L, Fleming M, Kriz R, Stahl M, Somers W, Fitz L, Mosyak L (2009) Protein Sci 18(3):569
36. Chothia C, Lesk AM (1986) EMBO J 5(4):823
37. Montelione GT, Zheng D, Huang YJ, Gunsalus KC, Szyperski T (2000) Nat Struct Biol 7(Suppl):982
38. Arnold K, Bordoli L, Kopp J, Schwede T (2006) Bioinformatics 22(2):195
39. Perrakis A, Tews I, Dauter Z, Oppenheim AB, Chet I, Wilson KS, Vorgias CE (1994) Structure 2(12):1169
40. van Aalten DM, Synstad B, Brurberg MB, Hough E, Riise BW, Eijsink VG, Wierenga RK (2000) Proc Natl Acad Sci USA 97(11):5842
41. Hollis T, Monzingo AF, Bortone K, Ernst S, Cox R, Robertus JD (2000) Protein Sci 9(3):544
42. Terwisscha van Scheltinga AC, Kalk KH, Beintema JJ, Dijkstra BW (1994) Structure 2(12):1181
43. Sun YJ, Chang NC, Hung SI, Chang AC, Chou CC, Hsiao CD (2001) J Biol Chem 276(20):17507
44. Terwisscha van Scheltinga AC, Armand S, Kalk KH, Isogai A, Henrissat B, Dijkstra BW (1995) Biochemistry 34(48):15619
45. van Aalten DM, Komander D, Synstad B, Gaseidnes S, Peter MG, Eijsink VG (2001) Proc Natl Acad Sci USA 98(16):8979
46. Bortone K, Monzingo AF, Ernst S, Robertus JD (2002) J Mol Biol 320(2):293
47. Garner AL, Gloeckner C, Tricoche N, Zakhari JS, Samje M, Cho-Ngwa F, Lustigman S, Janda KD (2011) J Med Chem 54(11):3963
48. Englebienne P, Moitessier N (2009) J Chem Inf Model 49(6):1568